Structural comparison of the *Caenorhabditis elegans* and human Ndc80 complexes bound to microtubules reveals distinct binding behavior

Elizabeth M. Wilson-Kubalek[a,*], Iain M. Cheeseman[b], and Ronald A. Milligan[a]
[a]Laboratory of Structure Cell Biology, Department of Integrative Structure and Computational Biology, Scripps Research Institute, La Jolla, CA 92037; [b]Whitehead Institute for Biomedical Research and Department of Biology, Massachusetts Institute of Technology, Cambridge, MA 02142

ABSTRACT **During cell division, kinetochores must remain tethered to the plus ends of dynamic microtubule polymers. However, the molecular basis for robust kinetochore–microtubule interactions remains poorly understood. The conserved four-subunit Ndc80 complex plays an essential and direct role in generating dynamic kinetochore–microtubule attachments. Here we compare the binding of the *Caenorhabditis elegans* and human Ndc80 complexes to microtubules at high resolution using cryo–electron microscopy reconstructions. Despite the conserved roles of the Ndc80 complex in diverse organisms, we find that the attachment mode of these complexes for microtubules is distinct. The human Ndc80 complex binds every tubulin monomer along the microtubule protofilament, whereas the *C. elegans* Ndc80 complex binds more tightly to β-tubulin. In addition, the *C. elegans* Ndc80 complex tilts more toward the adjacent protofilament. These structural differences in the Ndc80 complex between different species may play significant roles in the nature of kinetochore–microtubule interactions.**

Monitoring Editor
Kerry S. Bloom
University of North Carolina

Received: Dec 29, 2015
Revised: Feb 22, 2016
Accepted: Feb 23, 2016

INTRODUCTION

During cell division, the microtubule-based mitotic spindle forms direct connections with paired sister chromatids to capture and align them in the middle of the cell. Kinetochores assembled on sister chromatids are actively engaged with spindle microtubules during cell division. Kinetochore–microtubule attachments must be robust enough to harness the forces generated by microtubule dynamics and ensure chromosome motility. The conserved Ndc80 complex, a member of the KNL1/Mis12 complex/Ndc80 complex (KMN) network (Cheeseman *et al.*, 2006), is essential to generate and maintain robust kinetochore–microtubule attachments (Wigge and Kilmartin, 2001; McCleland *et al.*, 2004; DeLuca *et al.*, 2006; DeLuca and Musacchio, 2012) and is required for spindle checkpoint signaling (Martin-Lluesma *et al.*, 2002; DeLuca *et al.*, 2003; McCleland *et al.*, 2003). Although the Ndc80 complex is conserved throughout the vast majority of eukaryotes, the nature of the kinetochore–microtubule interface varies significantly between species. For example, whereas human kinetochores form at a single region on each chromosome, the nematode *Caenorhabditis elegans* is holocentric, forming kinetochores along the entire length of each chromosome (Maddox *et al.*, 2004). Similarly, the checkpoint kinase Mps1 detects the presence of kinetochore–microtubule attachments by binding to Ndc80 in human cells (Hiruma *et al.*, 2015; Ji *et al.*, 2015), but Mps1 is absent from *C. elegans* (Espeut *et al.*, 2015).

The Ndc80 complex is composed of Ndc80 (also known as HEC1 in humans; Chen *et al.*, 1997), Nuf2, Spc24, and Spc25. Structural studies demonstrated that the globular domains of Ndc80/Nuf2 and Spc24/Spc25 heterodimers are separated by coiled-coil stalks linked by a tetramerization domain, which gives this heterotetramer an overall ~57-nm-long, dumbbell-shaped architecture (Ciferri *et al.*, 2005; Wei *et al.*, 2005; Wang *et al.*, 2008). The Ndc80 complex binds to the microtubule lattice at an angle relative to the microtubule polarity, forming an arrowhead-like appearance (Wilson-Kubalek *et al.*, 2008). Although this complex is highly extended such that it can bridge the inner kinetochore with the microtubule plus

This article was published online ahead of print in MBoC in Press (http://www.molbiolcell.org/cgi/doi/10.1091/mbc.E15-12-0858) on March 3, 2016.

*Address correspondence to: Elizabeth M. Wilson-Kubalek (kubalek@scripps.edu).

Abbreviations used: CH domains, calponin homology domains; Cryo-EM, cryo-electron microscopy; 3D, three dimensional; EGTA, ethylene glycol tetraacetic acid; FSC, Fourier shell correlation; GTP, guanosine triphosphate; IHRSR, iterative helical real-space reconstruction; PIPES, 1,4-piperazinediethanesulfonic acid.

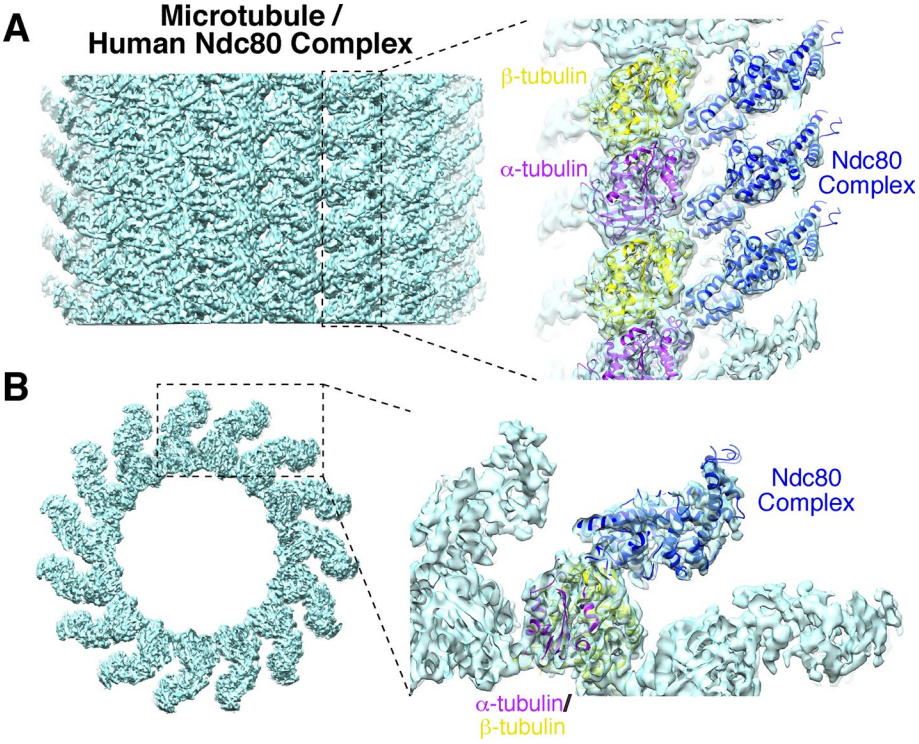

FIGURE 1: Surface rendering of the human Ndc80–bound microtubule complex. (A) The expanded boxed area shows a transparent single protofilament docked with the Ndc80 crystal structure (PDB ID 3IZ0; dark blue; Alushin *et al.*, 2010; Ciferri *et al.*, 2008) and the atomic model of tubulin (PDB ID 1JFF; α- and β-tubulin, purple and yellow, respectively; Lowe *et al.*, 2001). (B) Surface rendering of the axial view (blue) with boxed area expanded to show the docked crystal structures above.

end, there is a kink in the coiled-coil region ~16 nm from the globular microtubule-binding domains resulting from a "loop" in the secondary structure (Wang *et al.*, 2008). This allows the molecule to bend, which may aid in its interactions with microtubules. Recent work found that this conserved "loop" (Wang *et al.*, 2008) plays an essential role in protein–protein interactions by recruiting additional microtubule-binding proteins (Wang *et al.*, 2008; Hsu and Toda, 2011; Maure *et al.*, 2011).

Attachment of the Ndc80 complex to the microtubule in vivo and in vitro is dependent on the presence of the globular Ndc80–Nuf2 head and a disordered, positively charged N-terminal tail of the Ndc80 protein (Guimaraes *et al.*, 2008; Miller *et al.*, 2008), which interacts with the negatively charged carboxyl-terminal tails of tubulin (also known as E-hooks). A chimeric version of the human Ndc80 complex containing a minimal coiled-coil region, in which Ndc80 is fused to Spc25 and Nuf2 is fused to Spc24, has been studied by both x-ray crystallography and electron crystallography (Ciferri *et al.*, 2008; Alushin *et al.*, 2010, 2012). Based on previous cryo-EM studies, this shorter, 17-nm Ndc80 complex, named the Bonsai complex, binds identically to both α- and β-tubulin along a microtubule protofilament (Alushin *et al.*, 2010). In a more recent study, an important role was proposed for the Ndc80 tail domain in stabilizing lateral contacts between neighboring Ndc80^{Bonsai} complexes bound to the microtubule (Alushin *et al.*, 2012). In contrast, our previous lower-resolution structure of the *C. elegans* Ndc80 complex bound to microtubules showed unequal binding to α- and β-tubulin, with a predominant attachment to β-tubulin and a weaker association with α-tubulin along the protofilament (Wilson-Kubalek *et al.*, 2008).

To resolve these differences and define the molecular mechanisms by which the conserved Ndc80 complex associates with microtubules, we compared the binding of the *C. elegans* and human Ndc80 complexes to microtubules at comparable subnanometer resolution. We found that despite conserved sequences (Supplemental Figure S1A) and the conserved function of the Ndc80 complex, the nematode and human Ndc80 complexes have distinct binding and self-assembly modes on the microtubule.

RESULTS AND DISCUSSION

Human Ndc80 complex bound to microtubules

Full-length human Ndc80 complex is poorly behaved biochemically and difficult to purify at high concentrations. Therefore previous studies of the human Ndc80 complex bound to microtubules used the Ndc80^{Bonsai} complex (Alushin *et al.*, 2010, 2012), which binds to microtubules but lacks significant and potentially functionally relevant regions of Ndc80 downstream of its globular domain, including the "loop region," which has been shown to have a critical role at the microtubule-binding interface. To visualize the structural basis for the interaction of Ndc80 with microtubules, in this study we used a human Ndc80^{Broccoli} complex construct (Schmidt *et al.*, 2012), which contains the entire Ndc80 and Nuf2 microtubule-binding domains and downstream coiled-coil regions but lacks the Spc24/Spc25 domains.

We used cryo–electron microscopy (cryo-EM) to obtain a structure of microtubule–Ndc80^{Broccoli} complexes. The images were obtained using a K2 direct detector (Gatan, Pleasanton, CA) and the Krios microscope (FEI, Hillsboro, OR). To process the data, we used a single-particle approach and the iterative helical real-space reconstruction procedure (IHRSR; Egelman, 2007) with multimodel projection matching of microtubules with various numbers of protofilaments (Alushin *et al.*, 2014). A final refinement of the 15-protofilament microtubule segment alignment parameters was performed in FREALIGN (Sachse *et al.*, 2007), resulting in the highest-resolution three-dimensional (3D) reconstruction of the human Ndc80 complex to date, at 4.17-Å resolution (Fourier shell correlation [FSC] 0.143 criterion; Supplemental Figure S1B and Supplemental Table SS1). Our microtubule–Ndc80^{Broccoli} structure was at sufficient resolution to reveal secondary structure elements (Figure 1) and was similar to the 3D reconstruction of Ndc80^{Bonsai} complex generated previously (Alushin *et al.*, 2010). We found that the human Ndc80^{Broccoli} complex bound equivalently to α- and β-tubulin, consistent with the Alushin *et al.* (2010) structure. The atomic structure of the human Ndc80^{Bonsai} (Protein Data Bank [PDB] ID 3IZ0; Ciferri *et al.*, 2008; Alushin *et al.*, 2010) and tubulin (PDB ID 1JFF; Lowe *et al.*, 2001) fit well into our EM density map ($r \approx 0.9$; Figure 1). In addition, we observed density for the Ndc80 N-terminal tail, which is not present in the x-ray structure of soluble Ndc80 complex. Thus our analysis provides a high-resolution structure for the human Ndc80 complex bound to microtubules that is consistent with previous work, despite distinct constructs.

C. elegans Ndc80 complex bound to microtubules

Our previous structural analysis of the *C. elegans* Ndc80 complex bound to microtubules revealed a low-resolution structure (~30 Å; Wilson-Kubalek *et al.*, 2008), which prevented us from visualizing secondary structure elements. We therefore sought to generate a higher-resolution version of this structure using the *C. elegans* NDC-80/NUF2^{HIM-10} complex. We implemented the same strategy as before for the human Ndc80 complex. Preliminary 3D reconstructions for 13-, 14-, and 15-protofilament microtubules (unpublished data) indicated that the *C. elegans* Ndc80 complexes bound preferentially to the β-tubulin subunit, as we previously observed (Wilson-Kubalek *et al.*, 2008). However, we were not able to obtain high-resolution data for this complex due to incomplete decoration of the microtubules. This likely reflects the lower affinity of the *C. elegans* Ndc80 complex for microtubules compared with the human Nd8c0 complex (Schmidt *et al.*, 2012). Encouraged that this difference in the binding behavior of the human and *C. elegans* Ndc80 complexes was not due to the processing method, we evaluated various freezing strategies and increasing protein concentration to increase occupancy of the Ndc80 complexes on the microtubule. However, none of these attempts significantly improved the binding of the *C. elegans* Ndc80 complex to microtubules; instead, they resulted in a higher background of unbound protein.

We previously demonstrated that addition of *C. elegans* Ska1 complex improves the binding of the *C. elegans* Ndc80 complex to microtubules (Schmidt *et al.*, 2012). On mixing full-length *C. elegans* Ndc80 complex with full-length Ska1 complex before incubation with the microtubules, we observed a significant increase in fully decorated microtubules on the grid. To improve the resolution of *C. elegans* Ndc80 complex/Ska1 complex bound to microtubules, we collected a large cryo-EM data set using a direct detector and the Krios microscope. The resulting 3D reconstruction at subnanometer resolution of 4.06 Å (FSC 0.143 criterion; Supplemental Figure S1B and Supplemental Table SS1) revealed that these complexes preferentially bind to the β-tubulin monomer. The apparent stronger density in this region of the map produces a clear strong–weak binding pattern along the protofilament (Figure 2), with stronger binding to β-tubulin and weaker binding to α-tubulin. This result is similar to the preliminary 3D reconstruction of the microtubule–NDC-80/Nuf2^{HIM-10} complex in the absence of the Ska1 complex and to our previous report (Wilson-Kubalek *et al.*, 2008). Although there is no atomic structure of the *C. elegans* Ndc80 complex, the atomic structure of the human Ndc80^{Bonsai} structure fit well into our EM density map ($r \approx 0.8$), leaving no density to accommodate the Ska1 complex, indicating that Ska1 is too disordered to resolve in these reconstructions.

We previously showed that Ska1 decorates microtubules but does not associate with the microtubule in a specific orientation (Wellburn *et al.*, 2009). The apparent absence of the Ska1 complex is likely due to the averaging that occurs during image processing. Although the Ska1 density is not observed in the structure, the addition of the complex enabled us to produce a higher-resolution 3D reconstruction due to increased decoration of the Ndc80 complex on microtubules. Of importance, the addition of the Ska1 complex does not alter the structure of the Ndc80 complex on microtubules. Indeed, we obtained a similar 3D reconstruction of the full-length *C. elegans* Ndc80 complex bound to microtubules in the absence of Ska1, albeit at a lower resolution, 8.3 Å (FSC 0.5 criterion; Supplemental Table S1) due to incomplete decoration. We compared this map to the one with the full-length *C. elegans* Ndc80 complex in the presence of Ska1 complex (Figure 2) at a comparable resolution (Supplemental Figure S2, A–C). The maps are very similar at the threshold shown in Supplemental Figure S2. To verify that the full-length Ndc80 complex was not inhibiting access of the Ska1 complex to the microtubule interface due to the length and flexibility of the Ndc80 coiled-coils of the Spc24/25 domains, we also obtained a 3D reconstruction of the NDC-80/NUf2^{HIM-10} complex plus Ska1 complex bound to microtubules (Supplemental Table S1). The resulting map (unpublished data) was similar to that for the full-length Ndc80/ Ska1 complex.

Taken together, these results represent a subnanometer 3D reconstruction of the *C. elegans* Ndc80 complex bound to the microtubule interface and provide a means to directly compare our results with the human microtubule–Ndc80 complex structure.

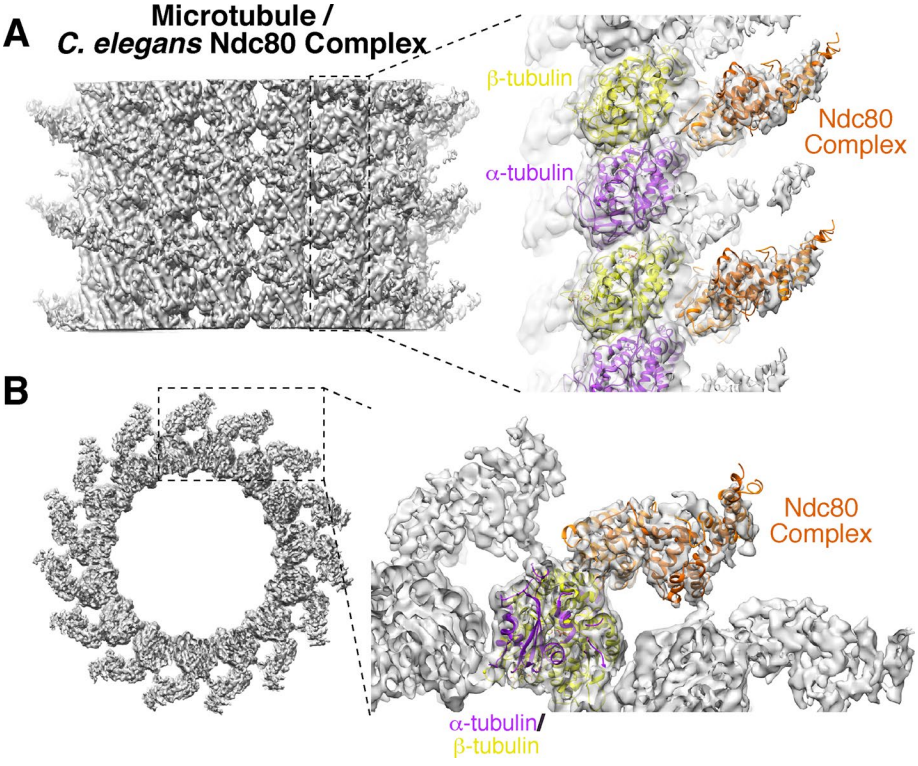

FIGURE 2: Surface rendering of the full-length *C. elegans* Ndc80 Complex plus Ska1 complex bound to microtubules. (A) The expanded boxed area shows a transparent single protofilament docked with the Ndc80 crystal structure (PDB ID 3IZ0; orange; Lowe *et al.*, 2001; Ciferri *et al.*, 2008; Alushin *et al.*, 2010) and the atomic model of tubulin (PDB ID 1JFF, α- and β-tubulin, purple and yellow, respectively; Lowe *et al.*, 2001), (B) Surface rendering of the axial view (gray) with boxed area expanded to show the docked crystal structures above.

Structural comparison of the human and *C. elegans* Ndc80 complexes

The raw data for both the human and *C. elegans* Ndc80 complexes were similar (Supplemental Figure S1C). After 3D processing, the differences became clear. The

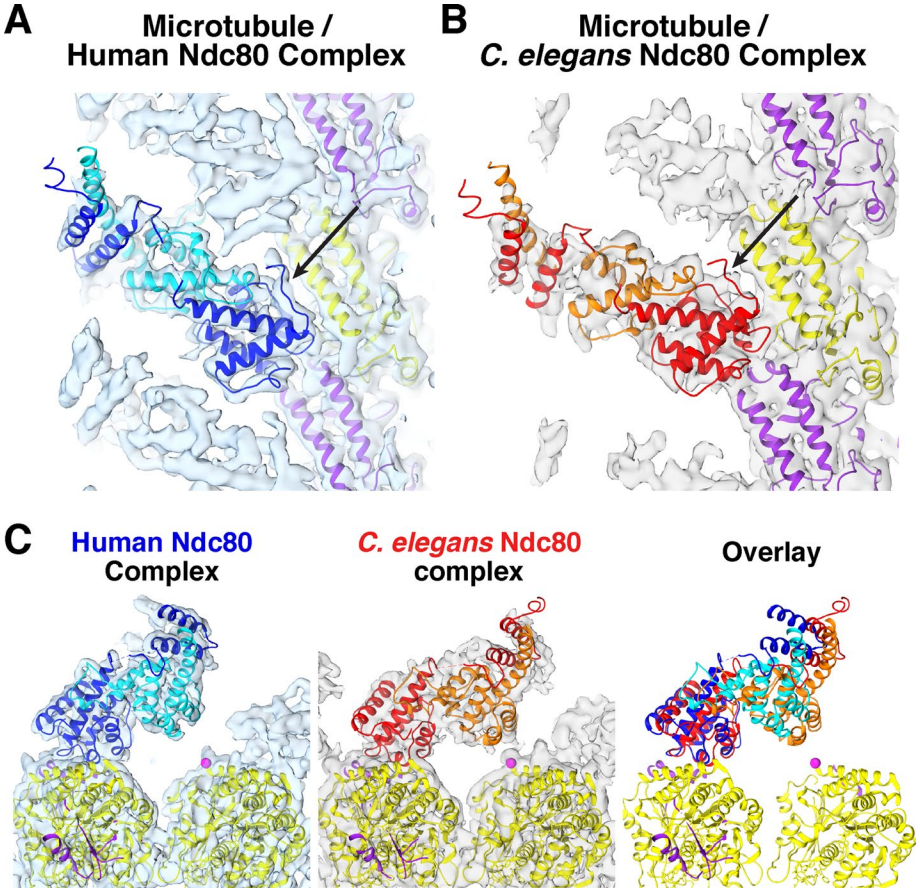

FIGURE 3: Structural comparison of the human and *C. elegans* Ndc80 complexes. (A) Single-protofilament view of the human Ndc80-bound microtubule complex (blue) and (B) the full-length *C. elegans* Ndc80-Ska1–bound microtubule (gray) showing the N-terminal domain (arrow). The Ndc80 crystal structure (PDB ID 3IZ0; Alushin *et al.*, 2010; Ciferri *et al.*, 2008) with dark blue Ndc80 and cyan Nuf2 in A and red Ndc80 and orange Nuf2 in B and the atomic model of tubulin (PDB ID 1JFF, with α- and β-tubulin in purple and yellow, respectively; Lowe *et al.*, 2001), (C) Axial views showing the proximity of the Nuf2 domain to the C-terminal domain of the neighboring β-tubulin (yellow). The pink sphere replaces the last amino acid of the C-terminal tail in the crystal structure. Right, superimposition of the same fit with atomic structures only.

human Ndc80^{Broccoli} complex bound equivalently to α- and β-tubulin, similar to the results of Alushin *et al.* (2010), whereas the full-length *C. elegans* Ndc80 complex displayed a distinct preference for β-tubulin (Wilson-Kubalek *et al.*, 2008). The unstructured N-terminal Ndc80 tail is not present in the x-ray structure but is resolved in our 3D map of the human microtubule–Ndc80^{Broccoli} complex (Figure 3A, arrow, and Supplemental Movie S1). In contrast, this density was weak and apparent only at higher thresholds in the map of the *C. elegans* complex (Figure 3B, arrow, and Supplemental Movie S1), suggesting that the N-terminal tail of *C. elegans* Ndc80 does not associate with microtubules in a regularly ordered manner. This differs from the human Ndc80 complex, which has been proposed to form attachments with neighboring Ndc80 complexes on adjacent protofilaments (Alushin *et al.*, 2010, 2012). By comparing the human and *C. elegans* reconstructions, we found that the *C. elegans* Ndc80 complex tilts ~20° more toward the neighboring protofilament than the human construct (Figure 3C). This additional tilt places the CH domain of Nuf2, which was previously identified as being important for microtubule binding in vitro (Ciferri *et al.*, 2008), closer to the C-terminal tail of β-tubulin and may allow more extensive interactions between the molecules (Alushin *et al.*, 2012).

The overall resolution of the full-length *C. elegans* Ndc80 complex and human Ndc80^{Broccoli} complex bound to microtubules was similar at 4.06 Å (FSC 0.143 criterion; Supplemental Figure S1B). The tubulin density in both maps was sufficiently resolved to clearly detect Taxol and surrounding loops (Figure 4, A and B). However, the density corresponding to Ndc80 was better-resolved in the human Ndc80^{Broccoli} map (Figures 3 and 4, C and D), suggesting that *C. elegans* Ndc80 could be more flexible and may require other proteins to keep it firmly attached to the microtubule polymer. It also remains possible that subtle differences in the primary sequence of tubulin (both between different species and in specific tubulin isoforms) or posttranslational modifications may further modulate the binding behavior of these complexes. Taken together, our data reveal that the binding mode of the Ndc80 complex is distinct between species, with different angles for their interaction with microtubules and differences in their ability to associate with every tubulin monomer.

Structural differences in Ndc80 complex–microtubule interactions between species might underlie distinct functional features

The Ndc80 complex is conserved across species and is the main facilitator of dynamic attachments between the kinetochore and microtubule plus ends. It is therefore surprising that the N-terminal tail, which is crucial for binding to the microtubule for the human protein, is highly divergent among species. The N-terminal tail domain of Ndc80 is essential for viability in human cells but is not essential in budding yeast (Guimaraes *et al.*, 2008; Miller *et al.*, 2008; Kemmler *et al.*, 2009) or *C. elegans* (Cheerambathur and Desai, 2014). The N-terminal tail of human Ndc80 plays a role in the reported cooperative binding behavior of the complex to microtubules, such that previous models suggested that the human Ndc80 complex oligomerizes along an individual microtubule protofilament (Alushin *et al.*, 2010, 2012). In contrast, the apparent strong/weak binding pattern suggests that the CH domains of the *C. elegans* Ndc80 complexes to adjacent tubulin monomers cannot be anchored to microtubules in this manner. This suggests that either Ndc80 oligomerization is not a conserved or critical functional property of the Ndc80 complex or other binding partners are required for robust binding of the *C. elegans* Ndc80 complex to spindle microtubules. Future studies of the specific interactions of the Ska1 complex with the Ndc80 complex and the microtubule surface will further our understanding of the different binding mechanisms between these species. Taken together, our results reveal that despite the strong functional conservation of the Ndc80 complex, its structural interaction with microtubules has evolved between species. The nature of these diverse binding interfaces is critical for considering structural and biophysical models for the mechanisms of Ndc80 complex interaction with microtubules and the basis by

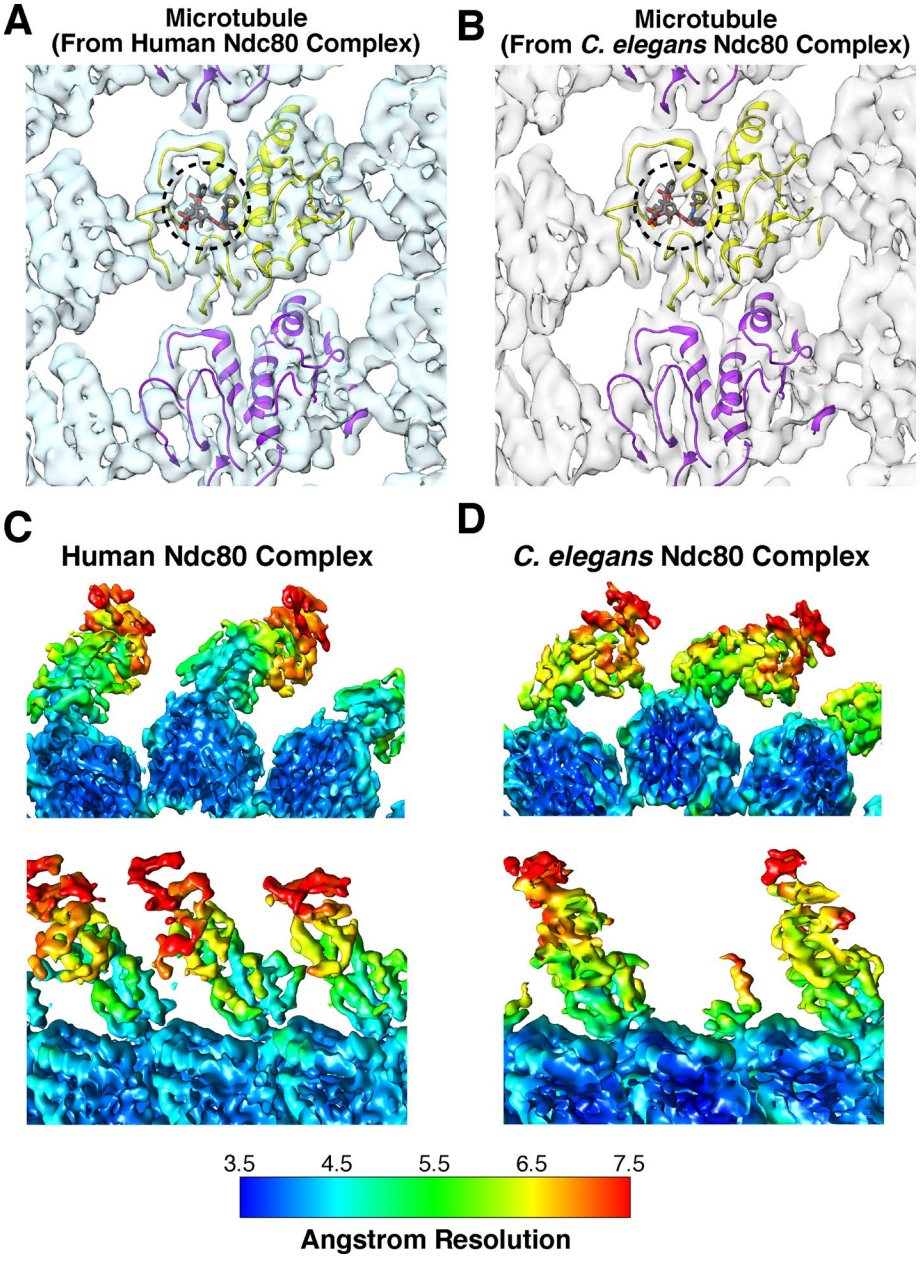

FIGURE 4: Local resolution calculation. (A, B) Taxol density observed in β-tubulin of maps of (A) human Ndc80–bound microtubule complex and (B) *C. elegans* Ndc80 complex plus Ska1 complex bound to microtubule. The Taxol density is highlighted in both maps with a dashed spherical outline. (C, D) The tubulin dimer and associated Ndc80 complex is colored according to its local resolution calculated using the bsoft blocres function. Dark blue density corresponds to 3.5-Å resolution, with a continuum of colors indicating increasingly lower resolution, ending with red at 7.5-Å resolution. The local resolution calculation reveals variability in resolution within the reconstructions, with the Ndc80 densities substantially less resolved than the tubulin density.

which kinetochores associate with and harness the force from depolymerizing microtubules to drive chromosome movement.

MATERIALS AND METHODS

Cryo-EM sample preparation

For grid preparation, full-length *C. elegans* Ndc80 complex and full-length *C. elegans* Ska1 complex (Schmidt *et al.*, 2012) were mixed in a 1:1 ratio at 6 μM. Human Ndc80^{Broccoli} complex (Schmidt *et al.*, 2012) was used at 3 μM. All proteins were present in BRB80 (80 mM 1,4-piperazinediethanesulfonic acid [PIPES], pH 6.8, 1 mM $MgCl_2$, 1 mM ethylene glycol tetraacetic acid [EGTA]). Bovine brain microtubules were prepared by polymerizing 5 mg/ml bovine brain tubulin (Cytoskeleton, Denver, CO) in polymerization buffer (80 mM PIPES, pH 6.8, 1 mM EGTA, 4 mM $MgCl_2$, 2 mM GTP, 12% dimethyl sulfoxide) for 30 min at 36° C. Paclitaxel was added at 250 μM before further incubation of 30 min at 36°C. The polymerized microtubules were then incubated at room temperature for several hours before use.

All microtubule samples were prepared on 400-mesh C-flat grids (Protochips, Morrisville, NC) containing 2.0-μm holes separated by 2.0-μm spacing. Grids were glow-discharged before sample application. The cryosamples were prepared using a manual plunger, which was placed in a homemade humidity chamber that varied between 80 and 90% relative humidity. A 4-μl amount of the microtubules at ~0.5 μM in 80 mM PIPES, pH 6.8, 4 mM $MgCl_2$, and 1 mM EGTA supplemented with 20 μM Taxol was allowed to absorb for 2 min, and then 4 μl of the Ndc80 preparations in BRB80 was added to the grid. After a short incubation of 2 min, the sample was blotted (from the back side of the grid) and plunged into liquid ethane.

Electron microscopy and image processing

Data were collected on the FEI Krios at the Scripps Research Institute or the FEI Krios at the University of California, Los Angeles. All images were recorded at 300 keV on a Gatan K2 direct electron detector with a pixel size of 1.31 Å at the specimen level using the automated Leginon software (Suloway *et al.*, 2005). Image processing was performed within the Appion processing environment (Lander *et al.*, 2009). The contrast transfer function was estimated by using CTFFIND3 (Mindell and Grigorieff, 2003), and the best-quality micrographs were selected for further processing. Microtubules were manually selected, and overlapping segments were extracted with a spacing of 80 Å along the filament. The boxed images were binned by a factor of two for two-dimensional analysis and 3D refinement. The particle stacks were subjected to iterative multivariate statistical analysis and multireference alignment. Particles in classes that did not clearly show Ndc80 density were excluded from further processing.

Cryo-EM 3D reconstruction

Undecorated 14- and 15-protofilament microtubule densities (Sui and Downing, 2010) were used as initial models for all preliminary reconstructions. We used the IHRSR procedure (Egelman, 2007) for multimodel projection matching of microtubule specimens with various numbers of protofilaments (Alushin *et al.*, 2014), using

libraries from the EMAN2 image processing package (Tang *et al.*, 2007). After each round of projection matching, an asymmetric back-projection is generated of aligned segments, and the helical parameters (rise and twist) describing the monomeric tubulin lattice are calculated. These helical parameters are used to generate and average 14 and 15 symmetry-related copies of the asymmetric reconstruction, and the resulting models were used for projection matching during the next round of refinement. In most reconstructions, we had a higher percentage of 15-protofilament segments. The resulting 14- and 15-protofilament reconstructions were similar, however; we used 15-protofilament segments only in the final refinement, since they do not have a seam, allowing for helical refinement. Final refinement of the 15-protofilament microtubule segment alignment parameters was performed in FREALIGN (Grigorieff, 2007) without further refinement of helical parameters. FSC curves were used to estimate the resolution of each reconstruction, using a cutoff of 0.143 (Supplemental Figure S1B). To estimate more accurately the resolution of each region of the reconstructed density, we performed a local resolution calculation using the blocres and blocfilt functions in the Bsoft processing package (Heymann and Belnap, 2007). This analysis revealed that the majority of the tubulin density is in the range of 3.5- to 5-Å resolution, whereas the Ndc80 portion ranges from 4.5- to 7.5-Å resolution (local resolution map; Figure 4, C and D). To better display the high-resolution features, we applied a *B*-factor of 100 Å^2, using the program bfactor (http://grigoriefflab.janelia.org). Atomic models were obtained through rigid-body docking of the electron crystallographic structure of tubulin (PDB ID 1JFF; Lowe *et al.*, 2001) and the Ndc80^{Bonsai} crystal structure (PDB ID 3IZ0; Ciferri *et al.*, 2008; Alushin *et al.*, 2010) into the cryo-EM density maps, using UCSF Chimera (Pettersen *et al.*, 2004).

Accession numbers

The Electron Microscopy Data Bank (EMDB) accession code for the human Ndc80:microtubule complex structure is EMD-6594. The EMDB accession code for the *C. elegans* Ndc80:microtubule complex structure is EMD-6595.

ACKNOWLEDGMENTS

We thank Gabe Lander (Scripps Research Institute) and Anchi Cheng (New York Structural Biology Center, New York, NY) for computational assistance and Gabe Lander, David Kern, and Julie Monda for critical reading of the manuscript. We are grateful to Hong Zhou, Xing Zhang, and Jiansen Jiang (Electron Imaging Center for Nanomachines, California NanoSystems Institute, University of California, Los Angeles, CA) for help with initial data collection and Jens Schmidt (University of Colorado, Boulder, CO) for generating some of the proteins used in this study. This project was funded by grants from the National Institutes of Health to R.A.M. and E.M.W.-K. (GM052468) and I.M.C. (GM088313).

REFERENCES

Alushin GM, Lander GC, Kellogg EH, Zhang R, Baker D, Nogales E (2014). High-resolution microtubule structures reveal the structural transitions in alphabeta-tubulin upon GTP hydrolysis. Cell 157, 1117–1129.

Alushin GM, Musinipally V, Matson D, Tooley J, Stukenberg PT, Nogales E (2012). Multimodal microtubule binding by the Ndc80 kinetochore complex. Nat Struct Mol Biol 19, 1161–1167.

Alushin GM, Ramey VH, Pasqualato S, Ball DA, Grigorieff N, Musacchio A, Nogales E (2010). The Ndc80 kinetochore complex forms oligomeric arrays along microtubules. Nature 467, 805–810.

Cheerambathur DK, Desai A (2014). Linked in: formation and regulation of microtubule attachments during chromosome segregation. Curr Opin Cell Biol 26, 113–122.

Cheeseman IM, Chappie JS, Wilson-Kubalek EM, Desai A (2006). The conserved KMN network constitutes the core microtubule-binding site of the kinetochore. Cell 127, 983–997.

Chen Y, Riley DJ, Chen PL, Lee WH (1997). HEC, a novel nuclear protein rich in leucine heptad repeats specifically involved in mitosis. Mol Cell Biol 17, 6049–6056.

Ciferri C, De Luca J, Monzani S, Ferrari KJ, Ristic D, Wyman C, Stark H, Kilmartin J, Salmon ED (2005). Architecture of the human ndc80-hec1 complex, a critical constituent of the outer kinetochore. J Biol Chem 280, 29088–29095.

Ciferri C, Pasqualato S, Screpanti E, Varetti G, Santaguida S, Dos Reis G, Maiolica A, Polka J, De Luca JG, De Wulf P, *et al.* (2008). Implications for kinetochore-microtubule attachment from the structure of an engineered Ndc80 complex. Cell 133, 427–439.

DeLuca JG, Gall WE, Ciferri C, Cimini D, Musacchio A, Salmon ED (2006). Kinetochore microtubule dynamics and attachment stability are regulated by Hec1. Cell 127, 969–982.

DeLuca JG, Howell BJ, Canman JC, Hickey JM, Fang G, Salmon ED (2003). Nuf2 and Hec1 are required for retention of the checkpoint proteins Mad1 and Mad2 to kinetochores. Curr Biol 13, 2103–2109.

DeLuca JG, Musacchio A (2012). Structural organization of the kinetochore-microtubule interface. Curr Opin Cell Biol 24, 48–56.

Egelman EH (2007). Single-particle reconstruction from EM images of helical filaments. Curr Opin Struct Biol 17, 556–561.

Espeut J, Lara-Gonzalez P, Sassine M, Shiau AK, Desai A, Abrieu A (2015). Natural loss of Mps1 kinase in nematodes uncovers a role for Polo-like kinase 1 in spindle checkpoint initiation. Cell Rep 12, 58–65.

Grigorieff N (2007). FREALIGN: high-resolution refinement of single particle structures. J Struct Biol 157, 117–125.

Guimaraes GJ, Dong Y, McEwen BF, Deluca JG (2008). Kinetochore-microtubule attachment relies on the disordered N-terminal tail domain of Hec1. Curr Biol 18, 1778–1784.

Heymann JB, Belnap DM (2007). Bsoft: image processing and molecular modeling for electron microscopy. J Struct Biol 157, 3–18.

Hiruma Y, Sacristan C, Pachis ST, Adamopoulos A, Kuijt T, Ubbink M, von Castelmur E, Perrakis A, Kops GJ (2015). Competition between MPS1 and microtubules at kinetochores regulates spindle checkpoint signaling. Science 348, 1264–1267.

Hsu KS, Toda T (2011). Ndc80 internal loop interacts with Dis1/TOG to ensure proper kinetochore-spindle attachment in fission yeast. Curr Biol 21, 214–220.

Ji Z, Gao H, Yu H (2015). Kinetochore attachment sensed by competitive Mps1 and microtubule binding to Ndc80. Science 348, 1260–1264.

Kemmler S, Stach M, Knapp M, Ortiz J, Pfannstiel J, Ruppert T, Lechner J (2009). Mimicking Ndc80 phosphorylation triggers spindle assembly checkpoint signalling. EMBO J 28, 1099–1110.

Lander GC, Stagg SM, Voss NR, Cheng A, Fellmann D, Pulokas J, Yoshioka C, Irving C, Mulder A, Lau PW, *et al.* (2009). Appion: an integrated, database-driven pipeline to facilitate EM image processing. J Struct Biol 166, 95–102.

Lowe J, Li H, Downing K, Nogales E (2001). Refined structure of alpha beta-tubulin at 3.5 A resolution. J Mol Biol 313, 1045–1057.

Maddox PS, Oegema K, Desai A, Cheeseman IM (2004). "Holo"er than thou: chromosome segregation and kinetochore function in elegans C. Chromosome Res 12, 641–653.

Martin-Lluesma S, Stucke VM, Nigg EA (2002). Role of Hec1 in spindle checkpoint signaling and kinetochore recruitment of Mad1/Mad2. Science 297, 2267–2270.

Maure JF, Komoto S, Oku Y, Mino A, Pasqualato S, Natsume K, Clayton L, Musacchio A, Tanaka TU (2011). The Ndc80 loop region facilitates formation of kinetochore attachment to the dynamic microtubule plus end. Curr Biol 21, 207–213.

McCleland ML, Gardner RD, Kallio MJ, Daum JR, Gorbsky GJ, Burke DJ, Stukenberg PT (2003). The highly conserved Ndc80 complex is required for kinetochore assembly, chromosome congression, and spindle checkpoint activity. Genes Dev 17, 101–114.

McCleland ML, Kallio MJ, Barrett-Wilt GA, Kestner CA, Shabanowitz J, Hunt DF, Gorbsky GJ, Stukenberg PT (2004). The vertebrate Ndc80 complex contains Spc24 and Spc25 homologs, which are required to establish and maintain kinetochore-microtubule attachment. Curr Biol 14, 131–137.

Miller SA, Johnson ML, Stukenberg PT (2008). Kinetochore attachments require an interaction between unstructured tails on microtubules and Ndc80(Hec1). Curr Biol 18, 1785–1791.

Mindell JA, Grigorieff N (2003). Accurate determination of local defocus and specimen tilt in electron microscopy. J Struct Biol 142, 334–347.
Pettersen EF, Goddard TD, Huang CC, Couch GS, Greenblatt DM, Meng EC, Ferrin TE (2004). UCSF Chimera—a visualization system for exploratory research and analysis. J Comput Chem 25, 1605–1612.
Sachse C, Chen J, Coureux P, Stroupe M, Fandrich M, Grigorieff N (2007). High-resolution electron microscopy of helical specimens: a fresh look at tobacco mosaic virus. J Mol Biol 371, 812–835.
Schmidt JC, Arthanari H, Boeszoermenyi A, Dashkevich NM, Wilson-Kubalek EM, Monnier N, Markus M, Oberer M, Milligan RA, Bathe M, *et al*. (2012). The kinetochore-bound Ska1 complex tracks depolymerizing microtubules and binds to curved protofilaments. Dev Cell 23, 968–980.
Sui H, Downing KH (2010). Structural basis of interprotofilament interaction and lateral deformation of microtubules. Structure 18, 1022–1031.
Suloway C, Pulokas J, Fellmann D, Cheng A, Guerra F, Quispe J, Stagg S, Potter CS, Carragher B (2005). Automated molecular microscopy: the new Leginon system. J Struct Biol 151, 41–60.
Tang G, Peng L, Baldwin PR, Mann DS, Jiang W, Rees I, Ludtke SJ (2007). EMAN2: an extensible image processing suite for electron microscopy. J Struct Biol 157, 38–46.
Wang HW, Long S, Ciferri C, Westermann S, Drubin D, Barnes G, Nogales E (2008). Architecture and flexibility of the yeast Ndc80 kinetochore complex. J Mol Biol 383, 894–903.
Wei RR, Sorger PK, Harrison SC (2005). Molecular organization of the Ndc80 complex, an essential kinetochore component. Proc Natl Acad Sci USA 102, 5363–5367.
Wellburn J, Grishchuk E, Backer C, Wilson-Kubalek E, Yates Jr, Cheeseman I (2009). The human kinetochore Ska1 complex facilitates microtubule depolymerization-coupled motility. Dev Cell 16, 374–385.
Wigge PA, Kilmartin JV (2001). The Ndc80p complex from Saccharomyces cerevisiae contains conserved centromere components and has a function in chromosome segregation. J Cell Biol 152, 349–360.
Wilson-Kubalek EM, Cheeseman IM, Yoshioka C, Desai A, Milligan RA (2008). Orientation and structure of the Ndc80 complex on the microtubule lattice. J Cell Biol 182, 1055–1061.